ORGANOMETALLICS
Article
pubs.acs.org/Organometallics

# Ultrafast Electron Transfers in Organometallic Supramolecular Assemblies Built with a NIR-Fluorescent Tetrabenzoporphyrine Dye and the Unsaturated Cluster $Pd_3(dppm)_3(CO)^{2+}$

Peng Luo,[†] Paul-Ludovic Karsenti,[†] Gessie Brisard,[†] Benoit Marsan,*[,‡] and Pierre D. Harvey*[,†]

[†]Département de Chimie, Université de Sherbrooke, Sherbrooke, QC J1K 2R1, Canada
[‡]Département de Chimie, Université du Québec à Montréal, Montréal, QC H2X 2J6, Canada

Supporting Information

**ABSTRACT:** The sodium 9,18,27,36-tetra-(4-carboxyphenylethynyl)tetrabenzoporphyrinatozinc(II) (**TCPEBP**) and sodium 5,10,15,20-tetra-(4-carboxyphenylethynyl)porphyrinatozinc(II) (**TCPEP**, for comparison purposes) salts were prepared to investigate the ionic driven host−guest assemblies made with the unsaturated redox-active cluster $Pd_3(dppm)_3(CO)^{2+}$ ($[\mathbf{Pd_3}^{2+}]$, dppm = $Ph_2PCH_2PPh_2$ as a $PF_6^-$ salt). Nonemissive dye···$[\mathbf{Pd_3}^{2+}]_x$ assemblies ($x$ = 1−4) are formed in methanol with $K_{1x}$ (binding constants) values of 83 200 (**TCPEBP**) and 70 400 $M^{-1}$ (**TCPEP**; average values extracted from graphical methods (Benesi−Hildebrand, Scott, and Scatchard), matching those obtained from fluorescence quenching experiments (static model)). These values are consistent with the more electron rich **TCPEBP** dye. This conclusion is corroborated by electrochemical data, which indicate a lower oxidation potential of the **TCPEBP** dye (+0.46 V) vs **TCPEP** (+0.70 V vs SCE) and by shorter calculated average Pd···O distances (DFT (B3LYP): 3.259 vs 3.438 Å, respectively). Using the position of the 0−0 component of the Q-bands and the electrochemical data, the excited-state driving forces for dye*···$[\mathbf{Pd_3}^{2+}]_x$ → dye$^{+\bullet}$···$[\mathbf{Pd_3}^{+\bullet}][\mathbf{Pd_3}^{2+}]_{x-1}$ are estimated for **TCPEBP** (+1.22 V vs SCE) and **TCPEP** (1.08 V vs SCE). The time scale for this process occurs within the laser pulse (fwhm <75−110 fs) during the measurements of the femtosecond transient absorption spectra. Conversely, the back electron transfers (dye$^{+\bullet}$···$[\mathbf{Pd_3}^{+\bullet}][\mathbf{Pd_3}^{2+}]_{x-1}$ → dye···$[\mathbf{Pd_3}^{2+}]_x$) occur well within 1 ps (respectively 650 and 170 fs for **TCPEBP** and **TCPEP**). Arguments are provided that the reorganization energy governs this difference.

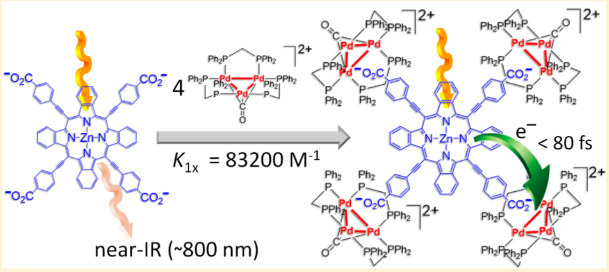

## INTRODUCTION

The rates for photoinduced electron transfers from dyads composed of carboxyphenyl-containing porphyrin dyes linked to the surface of $TiO_2$ nanoparticles are very fast (<100 fs up to 420 ps).[1] This property bears an obvious incidence of the overall efficiency of dye-sensitized solar cells (DSSCs).[2] Knowing that thermodynamic parameters control the size of these rates, the latter's are unavoidably bound to their molecular structures (i.e., singlet-state manifold energies, oxidation potentials, and excited-state driving forces). As more recently pointed out, absorbing more photons, particularly exploiting the near-IR region (NIR; 750−950 nm), is another parameter sought in solar cells. Obviously, shifting the absorption bands to the NIR is easily achieved by extending the $\pi$-system of the chromophore. In comparison with ZnTPP (5,10,15,20-tetraphenylporphyrinatozinc(II); $\lambda_{max}$(Q-band) ≈ 580 nm), a particularly efficient way to expand the $\pi$-system is to introduce ethynyl groups between the $C_{meso}$ and the phenyl groups.[3] In this case (i.e., 5,10,15,20-tetra(4-phenylethynyl)porphyrinatozinc(II)), the Q-band is shifted to nearly ∼680−700 nm.[3] Although this zinc(II)porphyrin-containing motif is relatively common,[4] and several photophysical and electrochemical investigations exist,[5] there is no study on the photoinduced electron transfer. Moreover, the title compound **TCPEP** (Chart 1) was previously reported in the context of preparing MOFs (metal−organic frameworks; note that in this case the 0−0 peak is reported at 687 nm in DMF), but no photophysical study was performed.[6] Another approach to extend the $\pi$-system, and therefore move the electronic spectra to the red region, is to fuse benzene rings onto the porphyrin chromophore.[7] By doing so, the 0−0 component moves to 737 nm (in THF). As the absorption band desirably shifts to the NIR, the singlet-state energy decreases proportionally, thus affecting the excited-state driving force for electron transfer.

In the context of this work, we recently reported assemblies of the type dye···$[\mathbf{Pd_3}^{2+}]_x$ (dye = **MCP**, 5-(4-carboxylphenyl)-10,15,20-tristolyl(porphyrinato)zinc(II), **DCP**, 5,15-bis(4-carboxylphenyl)-15,20-bistolyl(porphyrinato)zinc(II)), which exhibit smaller binding constants ($K_{1x}$ = 19 300 (**MCP**) and 22 000 $M^{-1}$ (**DCP**, $x$ = 1, 2)).[8] The choice of $Pd_3(dppm)_3(CO)^{2+}$ ($[\mathbf{Pd_3}^{2+}]$, dppm = $Ph_2PCH_2PPh_2$ as a $PF_6^-$ salt)[9] as the electron acceptor is based on the low

**Received:** January 20, 2016

Chart 1. Structures of $[\mathrm{Pd_3}^{2+}]$, TCPEBP, and TCPEP

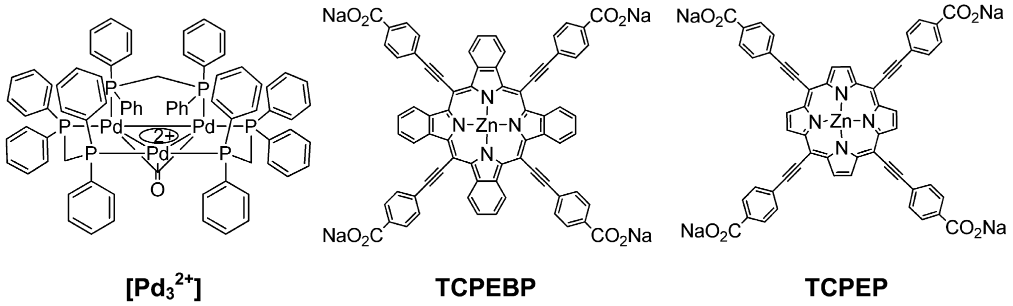

Scheme 1. Initial Synthetic Route of TCPEBP-2[a]

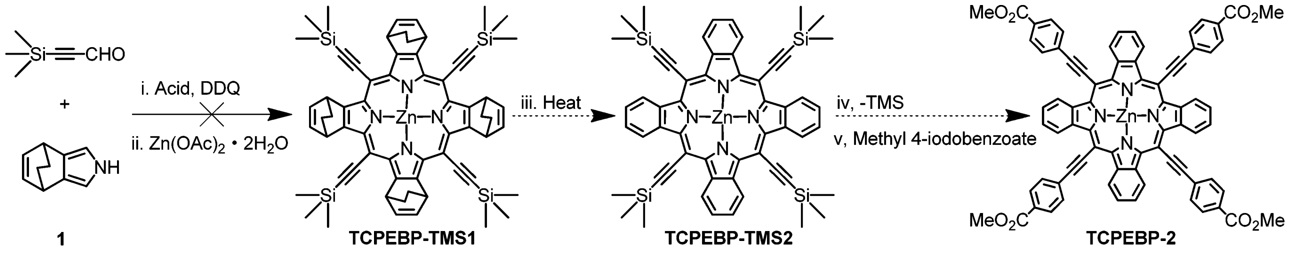

[a]This approach was unsuccessful.

Scheme 2. Synthetic Route for TCPEBP[a]

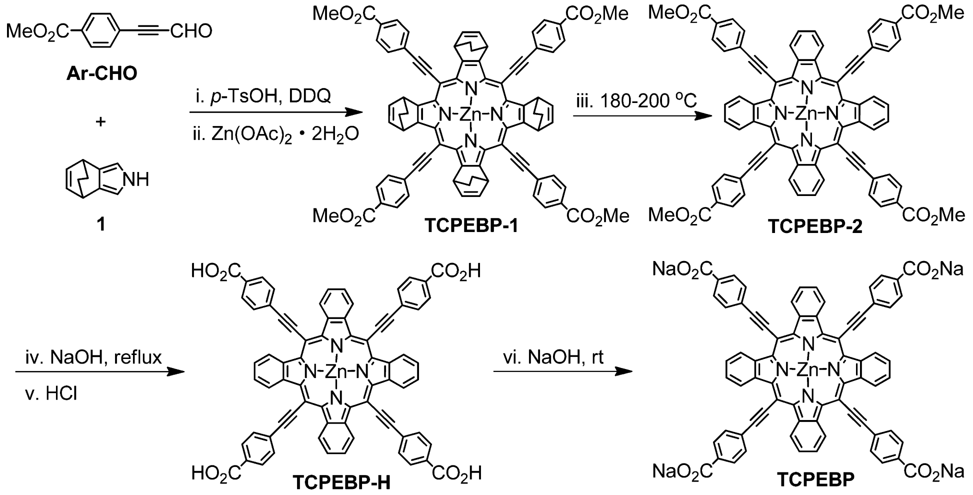

[a]Reagents and conditions: (i) *p*-TsOH, −40 °C to rt, 4 h, DDQ; (ii) $\mathrm{Zn(OAc)_2{\cdot}2H_2O}$, rt, overnight, overall yield for (i) and (ii) 5%; (iii) 180−200 °C, 10 min, 91%; (iv) NaOH, reflux, 5 h; (v) HCl, overall yield for (iv) and (v) 82%; (vi) NaOH, rt, overnight, 72%.

reduction potentials[10] and its well-known host guest behavior to bind carboxylates in a purely ionic manner.[11,12] Noteworthy, the photoinduced oxidative electron transfer occurs in a time scale < 85 fs in these two cases. We now report the dye··· $[\mathbf{Pd_3}^{2+}]_x$ assemblies where dye is either **TCPEBP** or **TCPEP**. The new compound **TCPEBP** is a NIR emitter and exhibits the largest $K_{1x}$ of this series. The dye···$[\mathbf{Pd_3}^{2+}]_x$ assemblies are found nonemissive as well, and the rates for electron transfer (dye*···$[\mathbf{Pd_3}^{2+}]_x$ → dye$^{+\bullet}$···$[\mathbf{Pd_3}^{+\bullet}][\mathbf{Pd_3}^{2+}]_{x-1}$) also occur within the laser pulse (fwhm < 75−110 fs).

## ■ RESULTS AND DISCUSSION

**Synthesis.** 4,7-Dihydro-4,7-ethano-2*H*-isoindole (**1**) has recently been reported to be an attractive synthon for the synthesis of tetrabenzoporphyrins because it could be easily oxidized to provide the target macrocycles in high yield compared to 4,5,6,7-tetrahydroisoindole or 4,7-dihydroisoindole.[13] On the basis of the typical method to incorporate acetylene groups into porphyrinic macrocycle, the synthesis approach illustrated in Scheme 1 was initially designed to synthesize **TCPEBP-2** as the key intermediate.[14] However, this approach leads to scrambling due to the high reactivity of 3-trimethylsilylpropynal, which tends to lose the trimethylsilyl groups under acid conditions and induces undesired polymerization. The MALDI-TOF spectra, indeed, confirmed the presence of **TCPEBP-TMS1**, but numerous unexplained secondary signals were also observed. Consequently, another synthetic strategy was employed.

Inspired by the first and sole synthesis of tetraethynyl-substituted tetrabenzoporphyrine, where direct condensation of **1** and phenylpropynal were applied,[7] the synthesis of the target dye was successfully achieved by utilizing aldehyde **Ar-CHO**, which can avoid the use of the "vulnerable" trimethylsilyl groups and introduce both ethynyl and carboxyl groups simultaneously (Scheme 2). The porphyrin macrocycle is generated using the classical acid catalysis condensation.[15] Then $Zn(OAc)_2{\cdot}2H_2O$ was employed to incorporate the zinc metal inside porphyrin to get **TCPEBP-1**. *p*-Toluenesulfonic acid (*p*-TsOH) used as a nonoxidizing organic acid gave a higher yield (5%) than common inorganic acids such as trifluoroacetic acid (1%) and boron trifluoride etherate (2%). It was expected that this condensation would show a lower yield compared to typical porphyrin condensation yields (20−30%) because of the delocalization of electronic density over aldehyde and ethynyl groups, which could increase the reactivity of aldehyde group and cause more side reactions. The intermediate **TCPEBP-1** was not stable, and **TCPEBP-2** can be prepared by retro-Diels−Alder reaction in the solid state upon heating. The intermediate **TCPEBP-2** was then hydrolyzed, and sodium salt was introduced by the neutralization of the acid groups using NaOH. The desired functional group $-CO_2^-$ promotes the desired ionic interactions with the $[\mathbf{Pd_3}^{2+}]$ cluster.

**Photophysical Characterization of the Dyes.** Prior to describing the properties of the targeted assemblies, some basic properties are provided. The electronic spectra of **TCPEBP** and **TCPEP** in methanol exhibit the typical $\pi\pi^*$ signature of the porphyrin chromophore (Figure 1 and Table 1), which is confirmed by DFT and TDDFT computations below. The fluorescence lifetimes, $\tau_F$, are 1.26 and 3.77 ns for **TCPEBP** and 2.61 and 3.59 ns for **TCPEP** in MeOH at 298 K and MeOH/2MeTHF (1:1) at 77 K, respectively (Table S1). The fluorescence quantum yields, $\Phi_F$, for **TCPEBP** and **TCPEP** in MeOH are 0.033 and 0.039 based on $H_2TPP$ ($\Phi_F = 0.11$).[16] These photophysical parameters are also reminiscent of that of the zinc(II)porphyrin chromophore, except that the **TCPEBP** chromophore emits in the NIR with maxima of the 0−0 component in the vicinity of 760 nm. The spectra signatures and $\tau_F$ data of **TCPEBP** are very similar to those of **TCPEBP-2** (SI).

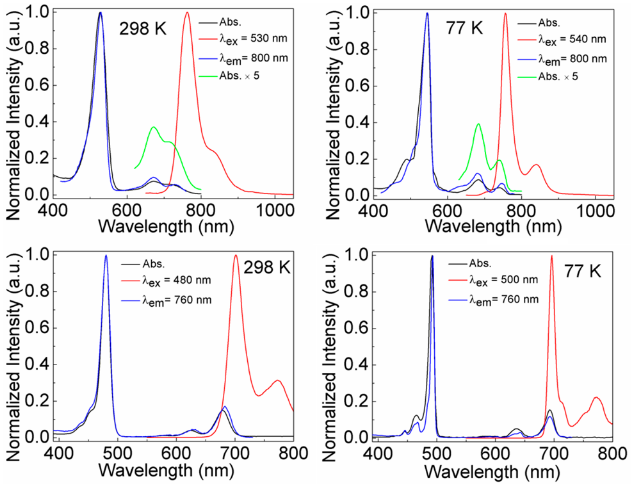

**Figure 1.** Top: Absorption (black), fluorescence (red), and excitation (blue) spectra of **TCPEBP** in MeOH at 298 K (left) and in MeOH/2MeTHF (1:1) at 77 K (right). Bottom: Absorption (black), emission (red), and excitation (blue) spectra of **TCPEP** in MeOH at 298 K (left) and in MeOH/2MeTHF (1:1) at 77 K (right).

**Cyclic Voltammetry and Driving Force for Electron Transfer.** Both dyes exhibit irreversible oxidation and reduction waves in the cyclic voltammograms (Figure 2), and the oxidation potentials are rather low (Table 2).

By using the 0−0 peaks of the Q-bands (at 77 K for more accuracy; 740 nm ($E^{0/*}$ = 1.68 eV) for **TCPEBP** and 695 nm ($E^{0/*}$ = 1.78 eV) for **TCPEP**) and the first oxidation peak potentials ($E^{0/+}$ = 0.46 and 0.70 V vs SCE for **TCPEBP** and **TCPEP**, respectively), the excited-state driving forces for oxidative electron transfer, $E^{*/+}$, can be evaluated (+1.22 and +1.08 V vs SCE for **TCPEBP** and **TCPEP**, respectively; modified Latimer diagram in Figure 2, right). Concurrently, $[\mathbf{Pd_3}^{2+}]$ exhibits a reduction potential $E^{0/-}$ = −0.50 V vs SCE.[17] The thermodynamic outcome is that the reactions dye*⋯$[\mathbf{Pd_3}^{2+}]_x \rightarrow$ dye$^{+\bullet}$⋯$[\mathbf{Pd_3}^{+\bullet}]_x$ are favorable ($\Delta E$ = +0.72 and +0.58 V vs SCE for dye = **TCPEBP** and **TCPEP**, respectively). Concurrently, using the reduction data for **TCPEBP** and **TCPEP** (Table 2) and the oxidation potential for $[\mathbf{Pd_3}^{2+}]$ ($E^{0/+}$ = +0.95 V vs SCE)[18] the excited-state driving forces for reduction electron transfer, $E^{*/-}$, can be evaluated (−0.70 and −0.67 V vs SCE for **TCPEBP** and **TCPEP**, respectively) as well as the $\Delta E$ for the reaction dye*⋯$[\mathbf{Pd_3}^{2+}]_x \rightarrow$ dye$^{-\bullet}$⋯$[\mathbf{Pd_3}^{3+\bullet}]_x$ (−0.70 + 0.95 = +0.25 and −0.67 + 0.95 = +0.28 V). These data indicate that oxidation quenching of the dye in the $S_1$ state is far more favorable than for the reduction. For comparison purposes, the reported $\Delta E$ values for *donor**⋯$[\mathbf{Pd_3}^{2+}] \rightarrow$ *donor*$^{+\bullet}$⋯$[\mathbf{Pd_3}^{\bullet+}]$ (+0.67; **MCP**, +0.72 V vs SCE; **DCP**)[8] are similar to those for **TCPEBP** and **TCPEP** (i.e., respectively +0.72 and +0.58 V vs SCE). This observation is expectedly consistent with the fact that the extension of the $\pi$-system decreases both the singlet-state energy and oxidation potential almost proportionally.

**DFT and TDDFT Computations.** The nature of the singlet excited states for both dyes have been addressed computationally. The frontier MOs exhibit the classic $\pi$-orbitals expected for porphyrins with extension of the atomic contributions into the ethynyl and fused benzene fragments (Figure 3). Further confirmations are obtained by calculating the positions of the spin-allowed transitions using TDDFT. The 100th transitions are placed in the SI, but the first four are included in Table 3. The positions of the lowest energy (doubly degenerate) transitions are computed at 679 and 713 nm for **TCPEP** and

**Table 1. Absorption, Emission, and Excitation Data for Porphyrinic Salts TCPEBP and TCPEP**

|  | T (K) | absorption $\lambda_{max}$ (nm) ($\varepsilon$ ($\times 10^3$ $M^{-1}{\cdot}cm^{-1}$)) | emission $\lambda_{max}$ (nm)[a] | excitation $\lambda_{max}$ (nm)[b] |
|---|---|---|---|---|
| **TCPEBP** | 298 | 529 (273.1), 676 (24.3), 727 (13.9) | 760 | 530 |
|  | 77 | 544, 686, 740 | 756 | 545 |
| **TCPEP** | 298 | 480 (248.8), 628 (5.4), 681 (25.6) | 699 | 482 |
|  | 77 | 491, 642, 695 | 696 | 492 |

[a] $\lambda_{exc}$ = 530 nm for **TCPEBP** at 298 K (in MeOH) and 540 nm at 77 K (in a MeOH/2MeTHF (1:1) mixture); 480 nm for **TCPEP** at 298 K and 500 nm at 77 K. [b] $\lambda_{em}$ = 800 nm for **TCPEBP** at 298 and 77 K; 760 nm for **TCPEP** at 298 and 77 K.

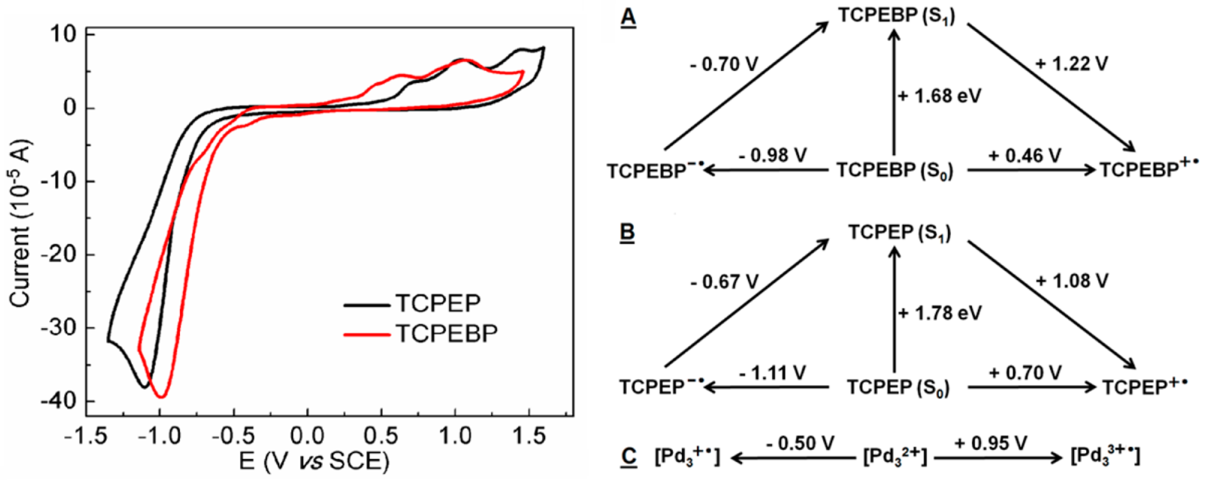

**Figure 2.** Left: Cyclic voltammograms of **TCPEBP** (red) and **TCPEP** (black) in MeOH ($3.0 \times 10^{-3}$ M) at 298 K containing 0.1 M $TBAPF_6$ as supporting electrolyte (scan rate = 50 mV/s). Right: Modified Latimer diagram for **TCPEBP** (A) and **TCPEP** (B) and Latimer diagram for [$\mathbf{Pd_3}^{2+}$] (C).

### Table 2. Oxidation ($E_{pa}$) and Reduction ($E_{pc}$) Peak Potentials of TCPEBP and TCPEP in MeOH

| | oxidation $E_{pa}$ (i.e., $E^{0/+}$) V vs SCE | reduction $E_{pc}$ (i.e., $E^{0/-}$) V vs SCE |
|---|---|---|
| **TCPEBP** | +0.46, +0.63, +1.09 | −0.98 |
| **TCPEP** | +0.70, +1.03, +1.43 | −1.11 |

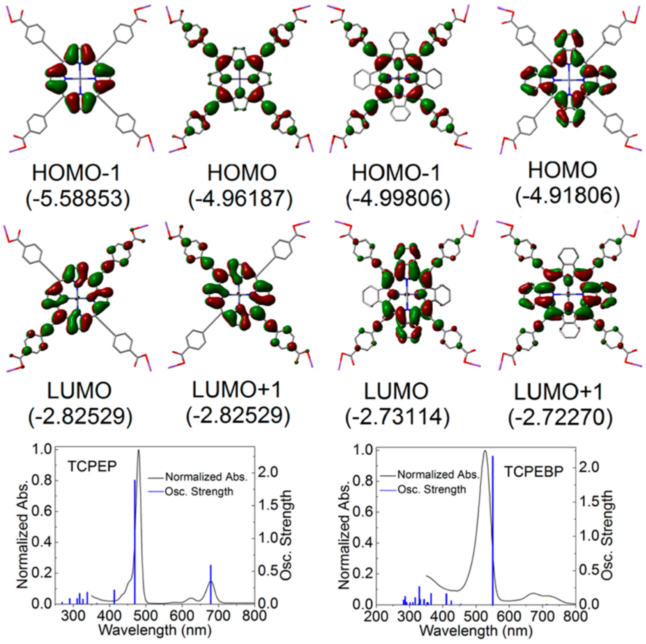

**Figure 3.** Top: Representations of selected frontier MOs of **TCPEP** (left) and **TCPEBP** (right) as $Na^+$ salts using a MeOH solvent field (energies in eV; for more frontier MOs, see SI). Bottom: Experimental UV−vis spectrum and oscillator strength for the 100th electronic transition of **TCPEP** (left) and **TCPEBP** (right) as $Na^+$ salts using a MeOH solvent field.

**TCPEBP**, respectively, and compare favorably to the corresponding experimental values at 681 and 727 nm (298 K). The calculated compositions of these transitions include the LUMO−1, LUMO, HOMO, and HOMO−1 as expected. Moreover, the computed positions of the 100th transition (blue bars in Figure 3, bottom) also compare favorably with the experimental spectra. Thus, the computations confirm the $\pi\pi^*$ nature of the lowest energy $S_1$ states.

### Table 3. Computed Positions, Oscillator Strengths, and Major Contributions for the First Four Electronic Transitions for TCPEP and TCPEBP (MeOH Solvent Field Applied)

| TCPEP | $\lambda$ (nm) | osc. strength | major contributions (%) |
|---|---|---|---|
| 1 | 679 | 0.5959 | H-1→L+1 (12), HOMO→LUMO (73), HOMO→L+1 (13) |
| 2 | 679 | 0.5961 | H-1→LUMO (12), HOMO→LUMO (13), HOMO→L+1 (73) |
| 3 | 469 | 1.8906 | H-1→LUMO (60), H-1→L+1 (20), HOMO→L+1 (10) |
| 4 | 469 | 1.8912 | H-1→LUMO (20), H-1→L+1 (60), HOMO→LUMO (10) |
| **TCPEBP** | **$\lambda$ (nm)** | **osc. strength** | **major contributions (%)** |
| 1 | 713 | 0.0119 | H-1→LUMO (47), HOMO→L+1 (52) |
| 2 | 712 | 0.0086 | H-1→L+1 (46), HOMO→LUMO (53) |
| 3 | 550 | 2.1583 | H-1→LUMO (53), HOMO→L+1 (47) |
| 4 | 550 | 2.176 | H-1→L+1 (54), HOMO→LUMO (46) |

**Evolution of the Absorption Spectra upon Addition of [$\mathbf{Pd_3}^{2+}$].** Additions of dyes into methanol solutions containing [$\mathbf{Pd_3}^{2+}$] lead to spectral modifications (Figure 4). For **TCPEP**, two isosbestic points are noted at 500 and 625 nm and exhibit the typical host−guest behavior for this cluster in the presence of a $-CO_2^-$ group.[11a] Typically, the strong [$\mathbf{Pd_3}^{2+}$] absorption shifts from 500 nm to 480 nm upon additions. For **TCPEBP**, this sought isosbestic point is not apparent because of the strong Soret band blurring the spectrum. However, clear evidence is provided below demonstrating the presence of this same host−guest behavior described by dye + $x$[$\mathbf{Pd_3}^{2+}$] ⇌ dye···[$\mathbf{Pd_3}^{2+}$]$_x$ ($x$ = 1−4).

Using three graphical methods, i.e., Benesi−Hildebrand, Scott, and Scatchard,[19] the binding constants $K_{1x}$ ($x$ = 1−4) have been determined (Table 4, and see graphs provided in Figure S1). The similarity of the extracted values for each method provides confidence in the data. Moreover, the fact that these graphs are linear and exhibiting the same slope over a large range of equivalents of [$\mathbf{Pd_3}^{2+}$], indicating that $K_{11} \approx K_{12}$

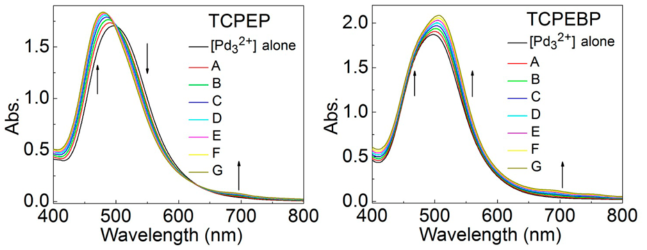

**Figure 4.** Left: Evolution of the absorption spectra of [$\mathbf{Pd_3^{2+}}$] ($9.72 \times 10^{-5}$ M) in MeOH at 298 K upon addition of **TCPEP** ($9.65 \times 10^{-6}$ M). Curves A−G were obtained with successive addition of 0.1 mL of the **TCPEP** solution. The arrows indicate the direction of absorption change with increasing **TCPEP**. Right: Evolution of the absorption spectra of [$\mathbf{Pd_3^{2+}}$] ($1.08 \times 10^{-4}$ M) in MeOH at 298 K upon addition of **TCPEBP** ($3.36 \times 10^{-6}$ M). Curves A−G were obtained with successive addition of 0.1 mL of the **TCPEBP** solution. The arrows indicate the direction of absorption change with increasing **TCPEBP**. Only certain initial spectra are shown for clarity.

**Table 4. Binding Constants for the Dye⋯[$\mathbf{Pd_3^{2+}}$]$_x$ Assemblies in MeOH at 298 K**

| | binding constants $K_{1x}$ (M$^{-1}$)[b] | | |
|---|---|---|---|
| substrate (average)[a] | Benesi−Hildebrand | Scott | Scatchard |
| **TCPEBP**⋯[$\mathbf{Pd_3^{2+}}$]$_x$ (83 200 M$^{-1}$) | 85 358 | 82 449 | 81 890 |
| **TCPEP**⋯[$\mathbf{Pd_3^{2+}}$]$_x$ (70 400 M$^{-1}$) | 75 016 | 67 784 | 68 495 |

[a]The values in parentheses are the average from the three methods. [b]The uncertainties are ∼±10% based on multiple measurements.

≈ $K_{13}$ ≈ $K_{14}$ for the assemblies dye⋯[$\mathbf{Pd_3^{2+}}$]$_x$ ($x \to 0, 1, 2, 3, 4$), means that the binding is not sterically nor electronically influenced by the sequential ionic anchoring of the clusters onto the dye. These constants, respectively 70 400 and 83 200 M$^{-1}$ for **TCPEP** and **TCPEBP** (average values), are consistent with the tetrabenzoporphyrin being a more electron-rich chromophore. These constants can be considered strong. The evolution of the absorption spectra of the dyes upon addition of [$\mathbf{Pd_3^{2+}}$] (Figure S2 in the SI) also exhibits spectral changes where the cluster band first appears as a shoulder near 480 nm but shifts to 500 nm when a large excess is added, meaning that all the binding sites are occupied and the amount of free [$\mathbf{Pd_3^{2+}}$] increases with further additions.

**Fluorescence Quenching Measurements.** These absorption spectral modifications are accompanied by a fluorescence quenching (Figure 5 as an example and the SI). However, the fluorescence lifetimes, $\tau_F$ (again 1.26 and 3.77 ns for **TCPEBP** and 2.61 and 3.59 ns for **TCPEP**, respectively, in MeOH at 298 K and MeOH/2MeTHF (1:1) at 77 K), remain constant for all [$\mathbf{Pd_3^{2+}}$] concentrations (data in Table S1). This behavior is strongly suggestive of a static quenching in both singlet states (eq 1):

$$\underset{\text{emissive}}{\mathbf{dye}^* + x[\mathbf{Pd_3^{2+}}]} \rightleftharpoons \underset{\text{nonemissive}}{\mathbf{dye}^*\cdots[\mathbf{Pd_3^{2+}}]_x\ (x = 1\text{–}4)} \qquad (1)$$

In order to confirm this process, the fluorescence quenching at 298 K is also graphically analyzed (Figure 5 for **TCPEBP** and SI for **TCPEP**). The absence of linearity in the Stern−Volmer plots (see graph in middle left) indicates that the mechanism is not dynamic quenching. The data are then analyzed using the relationship $\log[(\Phi_F^\circ - \Phi_F)/\Phi_F] = \log(K_b) + (n \log[\mathbf{Pd_3^{2+}}])$, where $\Phi_F^\circ$ and $\Phi_F$ are the fluorescence intensities respectively in the absence and presence of [$\mathbf{Pd_3^{2+}}$], $K_b$ is the binding constant, and $n$ is the average number of binding sites.[20] Values of $n$ = 3.85 (**TCPEP**) and 3.72 (**TCPEBP**) are evaluated (Table 5), and the fact that they approached the saturation value of 4 is fully consistent with the number of carboxylate sites on the chromophores.

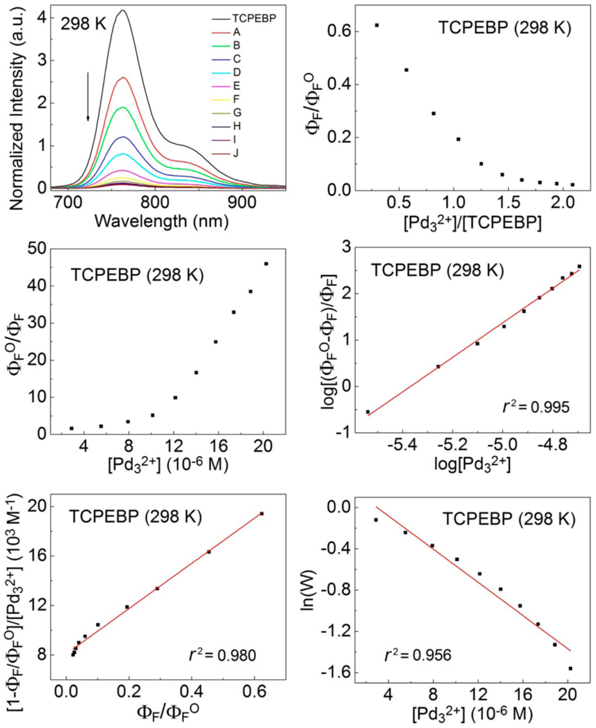

**Figure 5.** Top left: Evolution of the fluorescence spectra of **TCPEBP** ($9.71 \times 10^{-6}$ M) upon adding [$\mathbf{Pd_3^{2+}}$] in MeOH (298 K). Curves A−J were recorded with successive additions of 0.1 mL of [$\mathbf{Pd_3^{2+}}$] ($6.08 \times 10^{-5}$ M). Top right: Decrease of the relative fluorescence intensity ($\Phi_F/\Phi_F^\circ$) as a function of the [$\mathbf{Pd_3^{2+}}$]/[**TCPEBP**]. Middle left: Plot of ($\Phi_F^\circ/\Phi_F$) vs [$\mathbf{Pd_3^{2+}}$] (i.e., Stern−Volmer plot). Middle right: Graph of $\log[(\Phi_F^\circ - \Phi_F)/\Phi_F]$ vs $\log[\mathbf{Pd_3^{2+}}]$. Bottom left: graph of $[1 - (\Phi_F/\Phi_F^\circ)]/[\mathbf{Pd_3^{2+}}]$ vs ($\Phi_F/\Phi_F^\circ$). The two to three points curving out of the slope are due to the high concentration of clusters causing a deviation of the Beer−Lambert law. Bottom right: Graph of ln(W) vs [$\mathbf{Pd_3^{2+}}$] for the **TCPEBP**⋯[$\mathbf{Pd_3^{2+}}$]$_x$ assembly in MeOH (298 K).

**Table 5. Various Quenching Constants, $n$, $K_D$, and $V$, Extracted from the Fluorescence Quenching in MeOH at 298 K and in MeOH/2MeTHF (1:1) at 77 K**

| assembly (temperature) | $n$ | $K_D$ (M$^{-1}$) | $V$ (M$^{-1}$) |
|---|---|---|---|
| **TCPEBP**⋯[$\mathbf{Pd_3^{2+}}$]$_x$ (298 K) | 3.72 | 18 300 | 80 400 |
| **TCPEP**⋯[$\mathbf{Pd_3^{2+}}$]$_x$ (298 K) | 3.85 | 16 400 | 69 400 |
| **TCPEBP**⋯[$\mathbf{Pd_3^{2+}}$]$_x$ (77 K) | 3.61 | 19 300 | 81 000 |
| **TCPEP**⋯[$\mathbf{Pd_3^{2+}}$]$_x$ (77 K) | 3.76 | 18 700 | 72 600 |

In order to verify that the quenching is dominantly static, a mixed dynamic−static model was also used.[21] This graphical approach stems from a sphere of action model using the equation $[1 - (\Phi_F/\Phi_F^\circ)]/[\mathbf{Pd_3^{2+}}] = K_D(\Phi_F/\Phi_F^\circ) + (1 - W)/[\mathbf{Pd_3^{2+}}]$, where $W$ is the fraction of the excited-state quenching occurring from a collisional process given by $\exp(-V[\mathbf{Pd_3^{2+}}])$, where $V$ is the static quenching constant defining the volume of the sphere of action, and $K_D$ is the dynamic quenching constant. From a graph of $[1 - (\Phi_F/\Phi_F^\circ)]/[\mathbf{Pd_3^{2+}}]$ vs ($\Phi_F$/

$\Phi_F{}^{\circ}$), $K_D$ is obtained from the slope using a least-squares fit and the intercept leads to the $W$ values as a function of [$\mathbf{Pd_3}^{2+}$]. Then, $V$ is obtained from the slopes in the ln(W) vs [$\mathbf{Pd_3}^{2+}$] plots. These graphs are provided in Figure 5 for **TCPEBP** at 298 K. The remainder of the plots are placed in the SI.

These values are $K_D$ = 18 300 and $V$ = 80 400 for **TCPEBP···[$\mathbf{Pd_3}^{2+}$]$_x$**, $K_D$ = 16 400 $M^{-1}$, and $V$ = 69 400 $M^{-1}$ for **TCPEP···[$\mathbf{Pd_3}^{2+}$]$_x$**. Because the $V$ values are significantly larger than those for $K_D$, the static quenching dominates the overall mechanism. In addition, the $K_{1x}$ values (determined from absorption spectroscopy) are similar to those obtained for $V$ obtained from fluorescence quenching experiments as expected. In order to confirm this conclusion, this same analysis was performed on the assemblies' fluorescence at 77 K, where only static quenching is possible. The data are placed in the SI. Indeed, the $n$, $K_D$, and $V$ values are very similar at both temperatures (Table 5).

**DFT Calculation Results for Dye···[Pd$_3$$^{2+}$] Assemblies and Their MO Representations.** The geometries of the dye···[$\mathbf{Pd_3}^{2+}$] assemblies have been optimized by DFT computations. Only one anchored cluster was calculated for size reasons (Figure 6). The optimized geometries feature the anticipated long Pd···O distances generally associated with ionic interactions (selected data are placed in Table 6). The longer average Pd···O and Pd···Zn separations for **TCPEP** compared to **TCPEBP** are fully consistent with the smaller binding constants for **TCPEP···[$\mathbf{Pd_3}^{2+}$]** assemblies.

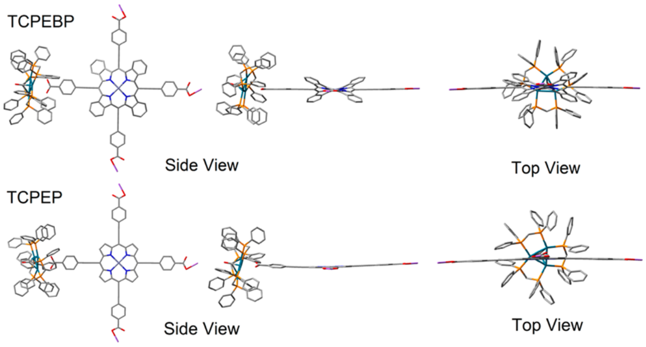

**Figure 6.** Optimized geometry of **TCPEBP···[$\mathbf{Pd_3}^{2+}$]** (top) and **TCPEP···[$\mathbf{Pd_3}^{2+}$]** (bottom) assemblies in MeOH solvent field.

The representations of the frontier MOs exhibit no atomic contribution on both the porphyrin dyes and [$\mathbf{Pd_3}^{2+}$] cluster for the same MO (Figure 7 for **TCPEBP** and the SI for **TCPEP**). This feature indicates that no MO coupling between the two fragments and that no electronic communication are favored. This expected conclusion supports that the interactions between the anion and cation are solely ionic in nature. The HOMO, HOMO−1, LUMO+1, and LUMO+2 for **TCPEBP···[$\mathbf{Pd_3}^{2+}$]** (Figure 7) and **TCPEP···[$\mathbf{Pd_3}^{2+}$]** (SI) are the same as analogues illustrated for the free dyes (above), indicating that these weak interactions do not alter the MO schemes of the chromophores.

**Table 6. Selected Distances for the Optimized Geometry of the TCPEBP···[Pd$_3$$^{2+}$] and TCPEP···[Pd$_3$$^{2+}$] Assemblies in the Ground State**

| | distances (Å) |
|---|---|
| **TCPEBP···[$\mathbf{Pd_3}^{2+}$]** | |
| Pd−Pd | 2.707, 2.695, 2.678 (av = 2.693) |
| Pd−P | 2.433, 2.411, 2.407, 2.396, 2.395, 2.392 (av = 2.406) |
| Pd···O | 1st O: 3.543, 3.213, 2.896 (av = 3.217); 2nd O: 3.696, 3.184, 3.023 (av = 3.301) |
| Pd···Zn | 15.181, 14.887, 14.642 (av = 14.903) |
| **TCPEP···[$\mathbf{Pd_3}^{2+}$]** | |
| Pd−Pd | 2.682, 2.675, 2.670 (av = 2.676) |
| Pd−P | 2.443, 2.413, 2.409, 2.408, 2.399, 2.380 (av = 2.409) |
| Pd···O | 1st O: 3.617, 3.438, 3.079 (av = 3.378); 2nd O: 3.868, 3.573, 3.056 (av = 3.499) |
| Pd···Zn | 15.582, 14.998, 14.956 (av = 15.179) |

The LUMO is composed of the in-plane dσ*(Pd−Pd) MO centered on the [$\mathbf{Pd_3}^{2+}$] cluster. This computational result is consistent with previous DFT calculations on the free cluster[22] and the cluster assembled with a dye.[8] This MO "insertion" of a cluster-localized MO within the four π and π* levels of the porphyrin dye is relevant, as it adds the possibility of electronic transitions between the filled frontier MOs of the dyes and this LUMO, although these are expected to be forbidden due to poor MO overlaps. As expected, the two lowest energy electronic transitions involve this dσ*(Pd−Pd) MO, and two π(dye*) → dσ*(Pd−Pd) transitions are computed (Table 7). For the upper energy electronic transitions, the calculated positions are very similar to that reported for the free dyes (above).

A reasonable match is noticed when comparing the graphs of the calculated positions and oscillator strengths of the first electronic transitions with the experimental spectra for both assemblies in MeOH (Figure 7). A blue-shift of ~30−50 nm of the calculated vs experimental positions of the pure electronic transitions is observed. The presence of a weak trailing tail at higher wavelengths from the Q-bands is obvious in the experimental spectra. These features extend all the way to 800 nm and a bit more. Thus, this match between calculations and experimental corroborates well the presence of assemblies in solutions.

**Relative Proportions of TCPEBP···[Pd$_3$$^{2+}$]$_x$ and TCPEP···[Pd$_3$$^{2+}$]$_x$.** Because the ionic interactions are generally weak, as corroborated by the binding constants in this work, the sufficient generation of assemblies must be controlled to secure reasonable amounts for the measurements of the transient absorption spectra. Their relative quantities have been estimated using both $K_{1x}$ (from absorption data, Table 4) and $V$ (from fluorescence quenching, Table 5) constants. These relative proportions are provided in Table 8, and the calculation procedure has been placed in the SI for convenience. In order to obtain a 1:2 [$CO_2^-$]/[$\mathbf{Pd_3}^{2+}$] ratio, it is necessary to use 1:8 equiv of dyes and cluster. By using the 1:2 [$CO_2^-$]/[$\mathbf{Pd_3}^{2+}$] ratio, >99% of the dyes are associated with at least one [$\mathbf{Pd_3}^{2+}$], and the major component is the dye···[$\mathbf{Pd_3}^{2+}$]$_4$ assemblies.

**Transient Absorption Spectra (TAS).** In the absence of fluorescence in the assemblies, this time-resolved methodology was used to evaluate the time scales for the singlet excited state quenching of the dyes by [$\mathbf{Pd_3}^{2+}$]. The unassociated cluster and dyes were first studied separately. The TAS of [$\mathbf{Pd_3}^{2+}$] were previously reported by us (SI of ref 8; it is provided as Figure S15 in the SI for convenience). It exhibit positive (bleach) and negative (transient) signals, respectively, at ~510 and ~410 nm, and the decay trace lies in the short picosecond time scale. No TAS signature of the cluster was observed in the spectra, indicating that its signal is rather weak in comparison with that of the dyes (i.e., strong bleached Soret band). The time evolution of the TAS of **TCPEP** is shown in Figure 8A, where an isosbestic point is depicted at ~490 and ~670 nm. The

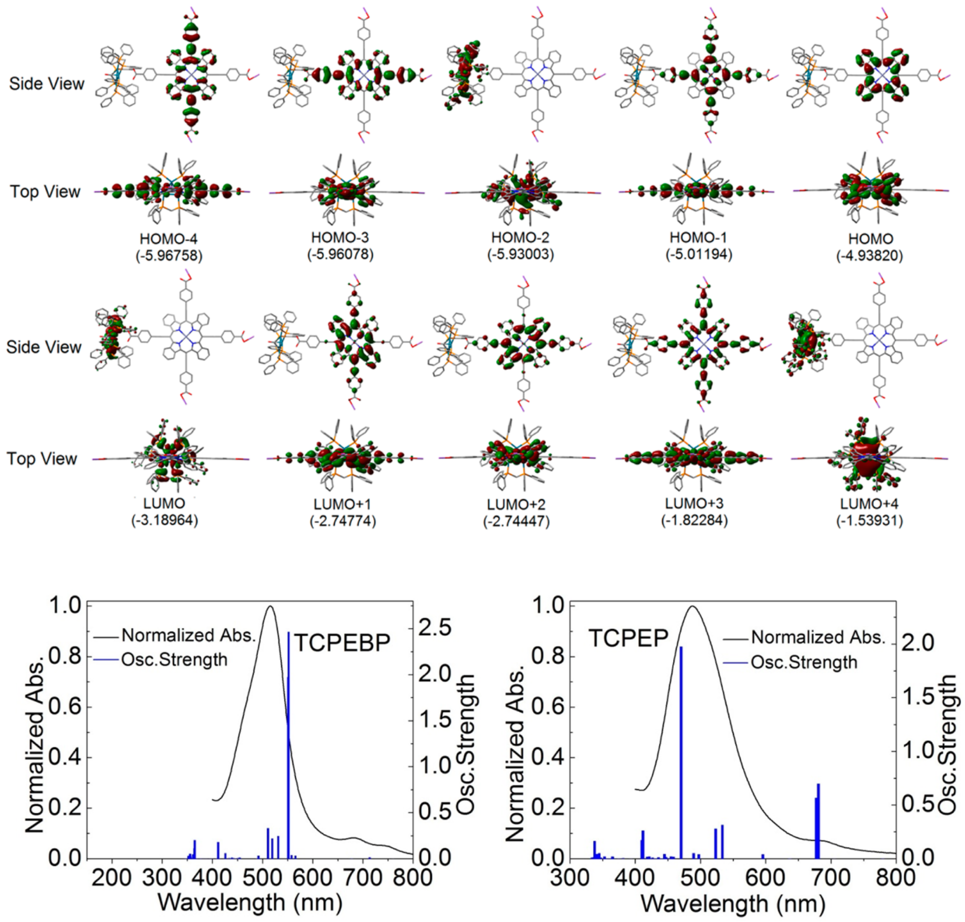

**Figure 7.** Top: Representations of the frontier MOs of the **TCPEBP···[Pd$_3^{2+}$]** assembly in a MeOH solvent field (energies in eV; see SI for those for **TCPEP···[Pd$_3^{2+}$]**). Bottom: Experimental UV−vis spectrum and oscillator strength for the 100th electronic transition of **TCPEBP···[Pd$_3^{2+}$]** (left; note the weak bar at 713 nm, detail shown in Table 7) and **TCPEP···[Pd$_3^{2+}$]** (right) as Na$^+$ salt using a MeOH solvent field. The 100th computed transitions are shown in the SI.

**Table 7. Computed Positions, Oscillator Strengths, and Major Contributions for the First Four Electronic Transitions for the TCPEBP···[Pd$_3^{2+}$] and TCPEP···[Pd$_3^{2+}$] and Assemblies (MeOH Solvent Field Applied)**

| no. | $\lambda$ (nm) | osc. strength | major contributions (%) |
|---|---|---|---|
| | | TCPEBP···[Pd$_3^{2+}$] | |
| 1 | 792 | 0 | HOMO→LUMO (100) |
| 2 | 761 | 0.0003 | H-1→LUMO (100) |
| 3 | 713 | 0.0154 | H-1→L+2 (44), HOMO→L+1 (49) |
| 4 | 713 | 0.0128 | H-1→L+1 (44), HOMO→L+2 (48) |
| TCPEP···[Pd$_3^{2+}$] | | | |
| 1 | 779 | 0.0015 | H-1→LUMO (91) |
| 2 | 705 | 0.0003 | HOMO→LUMO (98) |
| 3 | 681 | 0.6985 | H-2→L+2 (13), HOMO→L+1 (86) |
| 4 | 677 | 0.5653 | H-2→L+1 (14), HOMO→L+2 (86) |

**Table 8. Relative Percentage of Complexed Dyes in the 1:2 [CO$_2^-$]/[Pd$_3^{2+}$] Ratio Used for the Transient Absorption Spectra**

| [CO$_2^-$]/[Pd$_3^{2+}$] | assembly | %: $K_{1x}$, V | assembly | %: $K_{1x}$, V |
|---|---|---|---|---|
| 1:2 | TCPEBP···[Pd$_3^{2+}$]$_4$ | 87.8, 87.5 | TCPEP···[Pd$_3^{2+}$]$_4$ | 86.3, 86.7 |
| | TCPEBP···[Pd$_3^{2+}$]$_3$ | 10.7, 11.0 | TCPEP···[Pd$_3^{2+}$]$_3$ | 11.8, 11.6 |
| | TCPEBP···[Pd$_3^{2+}$]$_2$ | 1.29, 1.38 | TCPEP···[Pd$_3^{2+}$]$_2$ | 1.62, 1.54 |
| | TCPEBP···[Pd$_3^{2+}$] | 0.17, 0.17 | TCPEP···[Pd$_3^{2+}$] | 0.23, 0.19 |

deconvolution of the spectra indicates the presence of at least four species (Figure 8C). The easiest species to identify decays on the nanosecond time scale clearly associated with a triplet state, i.e., T$_1$, of the dye. This value is not accurate because of the delay line limited to about 8 ns. This T$_1$ species is rapidly generated in the 2−4 ps time scale, as noticed in the decay trace of the bleached signal at 480 nm (Figure 8E; purple trace) after exciting directly in the S$_1$ state (i.e., $\lambda_{\mathrm{exc}}$ = 680 nm) to minimize the number of possible species present in solution. Another species that is readily addressable decays with a 2.29 ns time constant. This value matches well the $\tau_F$ of 2.61 ns and is obviously associated with the S$_1$ species that are not associated with the cluster (Figure 8C, light green trace). The signal is weak with respect to that of the T$_1$ species, likely due to the efficient intersystem crossing, as suggested by the fast generation of this T$_1$ species (i.e., 2−4 ps).

A third species, decaying at ∼11 ps (turquoise trace), is also very weak and is tentatively assigned to an S$_1$ species similar to that encountered in solvent-induced vibrationally relaxed S$_1$ species commonly encountered in ZnTPP-containing chromophores.[23] These nonemissive S$_1$ species generally decay in the tens of picoseconds. A fourth species, also exhibiting a weak

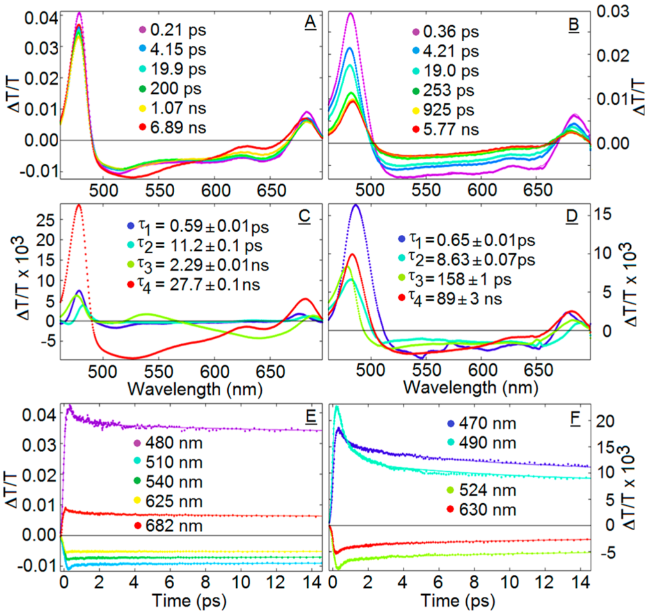

**Figure 8.** Top: Time evolution of the transient absorption spectra ($\lambda_{exc}$ = 680 nm; fwhm =107 fs) of free **TCPEP** (A) and the **TCPEP**⋯$[\mathbf{Pd_3}^{2+}]_x$ (B) assemblies in MeOH at 298 K ($\lambda_{exc}$ = 680 nm; fwhm = 107 fs). Middle: Deconvoluted spectra of transient species from the experimental spectra of free **TCPEP** (C) and the **TCPEP**⋯$[\mathbf{Pd_3}^{2+}]_x$ (D). Bottom: Rise times and decays measured at various wavelengths of free **TCPEP** (A) and the **TCPEP**⋯$[\mathbf{Pd_3}^{2+}]_x$ (B). The $[\mathrm{CO_2}^-]$/$[\mathbf{Pd_3}^{2+}]$ stoichiometry for the **TCPEP**⋯$[\mathbf{Pd_3}^{2+}]_x$ assemblies is 1:2. The positive signals are bleached bands, and the negative ones are transient absorptions.

intensity and decaying on the femtosecond time scale, is also deconvoluted, but its origin is not known with certainty. Its presence and assignment do not interfere with the conclusion.

The time evolution of the TAS of the **TCPEP**⋯$[\mathbf{Pd_3}^{2+}]_x$ assembly, in which the striking feature is a notable difference with the TAS of the free dye (**TCPEP**), is depicted in Figure 8B. This observation indicates that new products are formed in the presence of $[\mathbf{Pd_3}^{2+}]$. Quasi-isosbestic points are depicted at ~500 and ~670 nm, and the apparent final product is the **TCPEP** triplet species, as clearly observed by the comparison with the triplet species observed for the free dye (see red traces in Figure 8A–D). Again the nanosecond lifetime is unreliable due to the delay line. Because of the lower intensity of the triplet signals for the same dye concentration (i.e., ~3-fold), one concludes that the other product is the dye in its ground state. The two other species that are easily identified, based on comparison between the TAS of the dye in the absence of $[\mathbf{Pd_3}^{2+}]$, are the $S_1$ species (light green and turquoise traces in Figure 8C and D). While the 11.2 and 8.63 ps decays compare favorably, the decays for the 2.29 and 0.16 ns species do not. We do not have an explanation for this except that the extraction of each lifetime component in the time evolution in the TAS is generally challenging. We cannot attribute this difference to a quenching of the singlet state by electron transfer because the rise time for the formation of the charge-separated state should occur within the same time frame (i.e., 0.16 ns; see below). This was not the case.

Finally, the new species exhibits a significantly more intense, larger, and red-shifted signal (purple trace in Figure 8D compared to that in C) which features some fine structures in the 530–660 nm window. The fact that these two species labeled by purple traces decay with similar kinetics can only be coincidental. This major transient species (i.e., purple trace in Figure 8D) is the porphyrin cation. The key question is what the rise time is (i.e., rate of formation). The monitoring of this strong signal at 490 nm (turquoise trace in Figure 8F) indicates that a rise is occurring well within the excitation pulse. Conclusively, the charge-separated state (dye*⋯$[\mathbf{Pd_3}^{2+}]_x$ → dye$^{+\bullet}$⋯$[\mathbf{Pd_3}^{+\bullet}][\mathbf{Pd_3}^{2+}]_{x-1}$) is formed within 107 fs. All the other species, whether they concern the dye in the absence or in the presence of the cluster, are also formed within the pulse or in the 2–4 ps time window for the triplet species. The decay trace of the charge-separated species recovers with a kinetics of ~0.65 ps (i.e., back electron transfer (dye*⋯$[\mathbf{Pd_3}^{2+}]_x$ → dye$^{+\bullet}$⋯$[\mathbf{Pd_3}^{+\bullet}][\mathbf{Pd_3}^{2+}]_{x-1}$)).

The time evolution of the TAS of **TCPEBP** in the absence and presence of $[\mathbf{Pd_3}^{2+}]$ (A and B), the deconvoluted spectra of various species (C and D), and corresponding kinetic traces (E and F) are shown in Figure 9. These species behave somewhat similarly to that for **TCPEP** above, and only the differences and key features are described. The deconvoluted spectra of the free **TCPEBP** dye exhibit one more species, notably on the picosecond time scale, which disappear when $[\mathbf{Pd_3}^{2+}]$ is added. This behavior is consistent with the large binding constant for the **TCPEBP**⋯$[\mathbf{Pd_3}^{2+}]_x$ assembly, and free dye is essentially nonexistent (bottom of Table 8). The species with a 1.37 ns decay (purple trace in Figure 9C), which belongs to the unassociated **TCPEBP**, matches well the corresponding $\tau_F$ value (1.26 ns). More importantly, the species associated with the charge-separated state (dye$^{+\bullet}$⋯$[\mathbf{Pd_3}^{+\bullet}][\mathbf{Pd_3}^{2+}]_{x-1}$; purple trace in Figure 9D), readily recognizable from the multiple resolved features, exhibits the strongest signals, notably at 575

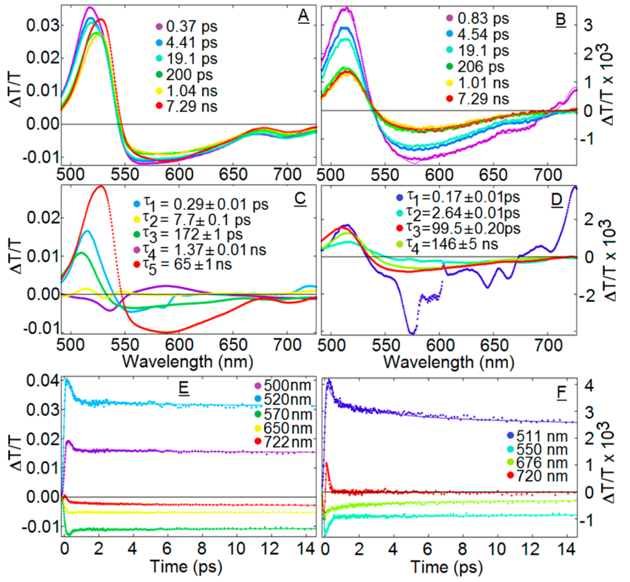

**Figure 9.** Top: Time evolution of the transient absorption spectra ($\lambda_{exc}$ = 720 nm; fwhm = 78 fs) of free **TCPEBP** (A) and the **TCPEBP**⋯$[\mathbf{Pd_3}^{2+}]_x$ (B) assemblies in MeOH at 298 K ($\lambda_{exc}$ = 720 nm). Middle: Deconvoluted spectra of transient species from the experimental spectra of free **TCPEP** (C) and the **TCPEBP**⋯$[\mathbf{Pd_3}^{2+}]_x$ (D). Bottom: Rise times and decays measured at various wavelengths of free **TCPEBP** (A) and the **TCPEBP**⋯$[\mathbf{Pd_3}^{2+}]_x$ (B). The $[\mathrm{CO_2}^-]$/$[\mathbf{Pd_3}^{2+}]$ stoichiometry for the **TCPEBP**⋯$[\mathbf{Pd_3}^{2+}]_x$ assemblies is 1:2. The positive and negative signals are bleached and transient bands, respectively.

and 720 nm (bleach). Again, the monitoring of the rise time indicates that all transients occur within the excitation pulse, here 78 fs. This is particularly evident for the signal at 720 nm (red trace in Figure 9F). So the charge-separated state occurs within this time frame, but also relaxes via a back electron transfer rather quickly (i.e., ~170 fs) in comparison to the **TCPEP** dye (~650 fs). At first glance, this result appears curious since the back electron transfer should even be more thermodynamically favorable for the **TCPEP** dye ($\Delta E$ = 1.20 (**TCPEP**) vs 0.96 V (**TCPEBP**) vs SCE; Figure 10), but the reorganization energies associated with these processes are bound to be different. Indeed, the presence of four fused benzene rings onto the porphyrin chromophore permits the positive charge to be spread over more C atoms than the **TCPEP** skeleton, thus making the reorganization energy (including both nuclear and solvent) smaller for **TCPEBP**. Such a situation would indeed render the electron transfers in **TCPEBP** assemblies more favorable.

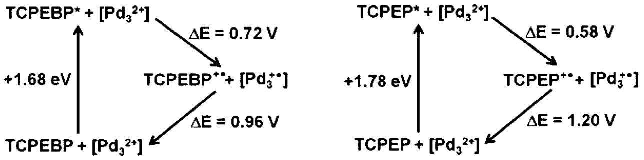

**Figure 10.** Thermodynamic parameters for the processes: $donor^{*}\cdots[\mathbf{Pd_3}^{2+}] \rightarrow donor^{+\bullet}\cdots[\mathbf{Pd_3}^{+\bullet}] \rightarrow donor\cdots[\mathbf{Pd_3}^{2+}]$ (this format is adopted instead of $\mathrm{dye}^{*}\cdots[\mathbf{Pd_3}^{2+}]_x \rightarrow \mathrm{dye}^{+\bullet}\cdots[\mathbf{Pd_3}^{+\bullet}][\mathbf{Pd_3}^{2+}]_{x-1} \rightarrow \mathrm{dye}^{*}\cdots[\mathbf{Pd_3}^{2+}]_x$ to simplify the drawing).

## CONCLUSION

By altering the structure of the dye going from **TCPEP** to the near-IR emitter **TCPEBP** (i.e., adding supplementary $\pi$-conjugation), unambiguously notable variations of the oxido-reduction potentials, $S_1$ energies, binding constants with [$\mathbf{Pd_3}^{2+}$], and excited-state driving forces for the oxidative quenching of the fluorescence ($\mathrm{dye}^{*}\cdots[\mathbf{Pd_3}^{2+}]_x \rightarrow \mathrm{dye}^{+\bullet}\cdots[\mathbf{Pd_3}^{+\bullet}][\mathbf{Pd_3}^{2+}]_{x-1}$), occur. However, for both assemblies, which exhibit strong binding constants, this efficient process is ultrafast (within the 75−110 fs time frame). The highly thermodynamically favorable back electron transfers ($\mathrm{dye}^{+\bullet}\cdots[\mathbf{Pd_3}^{+\bullet}][\mathbf{Pd_3}^{2+}]_{x-1} \rightarrow \mathrm{dye}^{*}\cdots[\mathbf{Pd_3}^{2+}]_x$) are also expectedly ultrafast (~170 and ~650 fs for **TCPEBP** and **TCPEP**, respectively). In the context of DSSCs, the fast injection of electrons into the conduction band of the $TiO_2$ nanoparticles by porphyrin-containing dyes has been demonstrated in the literature.[1] This behavior is also clearly corroborated in this work using the redox-active [$\mathbf{Pd_3}^{2+}$] cluster, but the noted ultrafast back electron transfer (<1 ps) potentially represents an obstacle not to be neglected among the many parameters for the design of these solar cells. This work demonstrates that a dye built upon the tetrabenzoporphyrin motif, and the tetraethynylphenylporphyrin as well, exhibits a serious possible thermodynamic/kinetic challenge to the photoinduced electron transfer.

## EXPERIMENTAL SECTION

**Materials.** All commercial reagents were used as received or purified by standard procedures before use. The $[Pd_3(dppm)_3(CO)](PF_6)_2$ cluster ([$\mathbf{Pd_3}^{2+}$]),[24a] 4,7-dihydro-4,7-ethano-2*H*-isoindole (**1**),[13a] and 5,10,15,20-tetra(4-carboxyphenylethynyl)-porphyrinatozinc(II) (**TCPEP-H**)[6,24b−d] were obtained according to literature procedures. 3-(4-Methoxycarbonylphenyl)prop-2-ynal (**Ar-CHO**)[24e] was synthesized using a modified method previously reported. Carboxylate sodium salts **TCPEBP** and **TCPEP** were further prepared from corresponding acid counterparts.[25]

**3-(4-Methoxycarbonylphenyl)prop-2-yn-1-ol (Ar-OH; Reaction Scheme S1 in the SI).** A mixture of methyl 4-iodobenzoate (4717 mg, 18.0 mmol), propargyl alcohol (2.1 mL, 36 mmol), $PdCl_2(PPh_3)_2$ (380 mg, 0.54 mmol), CuI (343 mg, 1.8 mmol), and $PPh_3$ (237 mg, 0.9 mmol) was refluxed under argon for 3 h in dry triethylamine (100 mL). After cooling the reaction mixture, the solvent was removed *in vacuo* and extracted with dichloromethane. The combined extracts were washed with water and dried over anhydrous $MgSO_4$. After removal of solvent *in vacuo*, the product was purified by silica column chromatography eluting with dichloromethane to give the title compound (2670 mg, 78%). $^1H$ NMR (400 MHz, $CDCl_3$-$d_3$): $\delta$ (ppm) 8.01−7.96 (d, *J* = 8 Hz, 2 H, Ar), 7.52−7.47 (d, *J* = 8 Hz, 2 H, Ar), 4.52 (s, 2 H, $CH_2$), 3.92 (s, 3 H, $CH_3$). MS (ESI): calcd for $C_{11}H_{10}O_3$ 190.0630, found 213.0522 (M + Na).

**3-(4-Methoxycarbonylphenyl)prop-2-ynal (Ar-CHO; Reaction Scheme S1 in the SI).** Pyridinium chlorochromate (12.94 g, 60 mmol) was added into a solution of compound **Ar-OH** (3800 mg, 20 mmol) in dry dichloromethane (100 mL), and then the mixture was stirred overnight at room temperature. Water was added to quench the reaction, and the mixture was extracted with dichloromethane. The combined extracts were washed with water and dried over anhydrous $MgSO_4$. After removal of solvent *in vacuo*, the product was purified by silica column chromatography eluting with dichloromethane to give compound **Ar-CHO** (1470 mg, 39%). $^1H$ NMR (400 MHz, $CDCl_3$-$d_3$): $\delta$ (ppm) 9.45 (s, 1 H, CHO), 8.09−8.05 (d, *J* = 8 Hz, 2 H, Ar), 7.70−7.65 (d, *J* = 8 Hz, 2 H, Ar), 3.95 (s, 3 H, $CH_3$). MS (ESI): calcd for $C_{11}H_8O_3$ 188.0473, found 243.0629 (M + Na + MeOH).

**9,18,27,36-Tetra(4-carboxymethylphenylethynyl)-3,6,12,15,21,24,30,33-octahydro-3,6;12,15;21,24;30,33-tetraethanotetrabenzoporphyrinatozinc(II) (TCPEBP-1).** (i) A stirred solution of **1** (1450 mg, 10 mmol) and **Ar-CHO** (1880 mg, 10 mmol) in 1 L of dry dichloromethane was added to *p*-toluenesulfonic acid monohydrate (190 mg, 1 mmol) under argon at −40 °C. After stirring for 3 h, the mixture was allowed to warm to room temperature and was stirred for an additional 1 h. Then 2,3-dichloro-5,6-dicyanobenzoquinone (DDQ, 2500 mg, 11 mmol) and 10 mL of triethylamine were added, and the reaction mixture was stirred for an extra 2 h. The solvents were removed *in vacuo*, and the residue was purified by column chromatography on alumina gel eluting with THF/DCM (1:9). The green fraction was collected, and the solvents were removed *in vacuo*. (ii) $Zn(OAc)_2{\cdot}2H_2O$ (2200 mg, 10 mmol) in 50 mL of MeOH was added to 200 mL of DCM solution of the above free-base porphyrin. The mixture was stirred overnight at room temperature. The solution was washed with water and brine and dried over anhydrous $Na_2SO_4$. The residue was purified by column chromatography on alumina gel eluting with THF/DCM (1:9). The crude product was collected as a green fraction and recrystallized with DCM/MeOH to yield the title compound (164 mg, 0.12 mmol, 5%). MS (MALDI-TOF): calcd for $C_{84}H_{60}N_4O_8Zn$ 1316.3703, found. 1316.4673 (M), 1288.4589 (M − $C_2H_4$), 1260.3977 (M − $C_4H_8$), 1232.3964 (M − $C_6H_{12}$), 1204.3179 (M − $C_8H_{16}$).

**9,18,27,36-Tetra(4-carboxymethylphenylethynyl)-tetrabenzoporphyrinatozinc(II) (TCPEBP-2).** **TCPEBP-1** (131 mg, 0.1 mmol) was heated in a sample tube under vacuum at 180−200 °C for 10 min. Then the solid was purified by column chromatography on silica gel eluting with dichloromethane and recrystallized with DCM/MeOH to yield the title compound (110 mg, 0.091 mmol, 91%). $^1H$ NMR (400 MHz, $CD_2Cl_2$-$d_2$): $\delta$ (ppm) 8.55−6.45 (m, 32 H, Ar and $\beta$-benzo), 4.16−3.87 (m, 12 H, $CH_3$). MS (MALDI-TOF): calcd for $C_{76}H_{44}N_4O_8Zn$ 1204.2451, found 1204.2230 (M).

**9,18,27,36-Tetra(4-carboxyphenylethynyl)tetrabenzoporphyrinatozinc(II) (TCPEBP-H).** An aqueous NaOH solution (5 M, 1 mL, 5.0 mmol) was added to a THF/MeOH (2:1) solution of **TCPEBP-2** (120 mg, 0.1 mmol, 60 mL). The mixture was stirred under reflux for 5 h. Then aqueous HCl solution (1 M) was carefully added to adjust the solution pH to 6−7. The resultant precipitate was filtered and washed with $H_2O$ and diethyl ether to afford the title compound (94 mg, 0.082 mmol, 82%). $^1$H NMR (400 MHz, DMSO-$d_6$): $\delta$ (ppm) 9.92 (s, 4 H, $CO_2H$), 8.80−7.11 (m, 32 H, Ar and $\beta$-benzo). MS (MALDI-TOF): calcd for $C_{72}H_{36}N_4O_8Zn$ 1148.1825, found 1148.2194 (M).

**Sodium 9,18,27,36-Tetra(4-carboxyphenylethynyl)-tetrabenzoporphyrinatozinc(II) (TCPEBP).** **TCPEBP-H** (115 mg, 0.1 mmol) was dissolved in 30 mL of THF under argon. Then 4.0 equiv of aqueous NaOH solution was added slowly, and the mixture was stirred overnight at room temperature. The resultant precipitate was filtered and washed with DCM, THF, and diethyl ether. The solid was dissolved in 50 mL of MeOH and filtered; then 30 mL of toluene was added into the filtrate. By carefully removing the MeOH *in vacuo*, the porphyrin salt was precipitated out of the solution. The resultant precipitate was filtered and washed with DCM and diethyl ether. After drying under vacuum, the title compound was obtained (88 mg, 0.072 mmol, 72%). IR (KBr): 2189 cm$^{-1}$ C≡C, 1571 cm$^{-1}$ C═O. $^1$H NMR (400 MHz, $CD_3OD$-$d_4$): $\delta$ (ppm) 8.52−8.25 (m, 16 H, Ar), 8.08−7.80 (m, 16 H, $\beta$-benzo).

**Sodium 5,10,15,20-Tetra(4-carboxyphenyl)ethynyl-porphyrinatozinc(II) (TCPEP).** **TCPEP-H** (95 mg, 0.1 mmol) was dissolved in 30 mL of DMF under argon. Then 4.0 equiv of aqueous NaOH solution was added slowly, and the mixture was stirred overnight at room temperature. The resultant precipitate was filtered and washed with DMF, THF, and diethyl ether. The solid was dissolved in 100 mL of MeOH and filtered. A 50 mL amount toluene was added into the filtrate. By carefully removing the MeOH *in vacuo*, the porphyrin salt was precipitated out of the solution. The resultant precipitate was filtered and washed with THF and diethyl ether. After drying under vacuum, the title compound was obtained (72 mg, 70%). IR (KBr): 2196 cm$^{-1}$ C≡C, 1595 and 1541 cm$^{-1}$ C═O. $^1$H NMR (400 MHz, $CD_3OD$-$d_4$): $\delta$ (ppm) 9.79 (s, 8 H, $\beta$), 8.31−8.06 (m, 16 H, Ar).

**Instruments.** NMR spectra were collected on a Bruker DRX 400 spectrometer using deuterated solvent with tetramethylsilane as internal standard. MALDI-TOF mass spectra were recorded on a Waters Synapt MALDI HDMS TOF mass spectrometer (Waters Canada, Ontario, Canada) powered by a solid-state laser with dithranol as matrix. All samples were freshly prepared and measured within 1 h. The IR spectra were acquired on a Bomem FT-IR MB series spectrometer equipped with a baseline-diffused reflectance. Absorption spectra were measured on a Varian Cary 300 Bio UV−vis spectrometer at 298 K and on a Hewlett-Packard 8452A diode array spectrometer with a 0.1 s integration time at 77 K. Steady-state fluorescence and excitation spectra were acquired on an Edinburgh Instruments FLS980 phosphorimeter equipped with single monochromators. NIR emission was measured by a QuantaMaster 400 phosphorimeter from Photon Technology International, which was excited by a xenon lamp and recorded with a NIR PMT-7-B detector. All fluorescence spectra were corrected for instrument response. Fluorescence lifetime measurements were made with the FLS980 phosphorimeter using a 378 nm picosecond pulsed diode laser (fwhm = 90 ps) as an excitation source. Phosphorescence lifetime measurements were acquired on the FLS980 using a microsecond flashlamp. Data collection on the FLS980 system is done by a time-correlated single photon counting system.

**Electrochemistry.** Electrochemical measurements were conducted with a three-electrode potentiostat (Princeton, Applied Research Corporation, model 273A) in solvents deoxygenated by purging with purified Ar gas. Cyclic voltammograms were obtained by using a three-electrode cell equipped with a glassy carbon disk (0.07 cm$^2$) as the working electrode, a platinum wire as auxiliary electrode, and a freshly polished silver wire as pseudoreference electrode at 298 K. The working electrode was polished with aluminum (0.03 $\mu$m) on felt pads (Buehler) and treated ultrasonically for 1 min before each experiment. The reproducibility of individual potential values was within ±5 mV. Tetra-*n*-butylammonium hexafluorophosphate ($TBAPF_6$) was used as supporting electrolyte, which was obtained from Sigma-Aldrich and used without further purification. Ferrocene/ferrocenium ($Fc/Fc^+$) was used as internal standard before and after each measurement (less than 1 h). Potentials were converted to values for saturated calomel electrode (SCE) by addition of 0.16 V, which was calibrated using $Fc/Fc^+$.

**Calculation Procedure.** All density functional theory (DFT) and time-dependent density functional theory (TDDFT) calculations were performed with Gaussian 09[26] at the Université de Sherbrooke with the Mammouth supercomputer supported by Le Réseau Québécois De Calculs Hautes Performances. The DFT geometry optimizations as well as TD-DFT calculations[27−36] were carried out using the B3LYP method. A 6-31G* basis set was applied to H, C, N, O, Na, and P atoms in porphyrins, palladium cluster, and porphyrin-palladium cluster assembly. Valence double $\zeta$ with SBKJC effective core potentials were used for all Zn and Pd atoms.[37−42] All calculations were carried out in a methanol solvent field. The calculated absorption spectra were obtained from GaussSum 2.1.[43]

**Femtosecond Transient Absorption Spectroscopy.** The fs transient spectra and decay profiles were acquired on a homemade system using the SHG of a Soltice (Spectra Physics) Ti-sapphire laser ($\lambda_{exc}$ = 398 nm; fwhm = 75 fs; pulse energy = 0.1 $\mu$J per pulse, repetition rate = 1 kHz; spot size ≈ 500 $\mu$m), a white light continuum generated inside a sapphire window, and a custom-made dual CCD camera of 64 × 1024 pixels sensitive between 200 and 1100 nm (S7030, Spectronic Devices). The delay line permitted probing up to 4 ns with an accuracy of ∼4 fs. The results were analyzed with the program Glotaran (http://glotaran.org), permitting extraction of a sum of independent exponentials ($I(\lambda,t) = C_1(\lambda) \times e^{-t_1/\tau} + C_2(\lambda) \times e^{-t_2/\tau} + \ldots$) that fits the whole 3D transient map.

## ■ ASSOCIATED CONTENT

### Ⓢ Supporting Information

The Supporting Information is available free of charge on the ACS Publications website at DOI: 10.1021/acs.organomet.6b00050.

Figures and tables giving fluorescence lifetimes, binding constants, UV−vis spectra evolutions, quenching constants, DFT and TDDFT calculations, relative percentage of complexed dyes, NMR, and MALDI-TOF (PDF)

## ■ AUTHOR INFORMATION

### Corresponding Authors

*E-mail: marsan.benoit@uqam.ca.
*E-mail: pierre.harvey@usherbrooke.ca.

### Notes

The authors declare no competing financial interest.

## ■ ACKNOWLEDGMENTS

This research was supported by the Natural Sciences and Engineering Research Council of Canada (NSERC), the Fonds de Recherche du Québec−Nature et Technologies (FRQNT), the Centre Québécois des Matériaux Fonctionnels (CQMF), and the Centre d'Études des Matériaux Optiques et Photoniques de l'Université de Sherbrooke (CEMOPUS).

## ■ REFERENCES

(1) (a) Ye, S.; Kathiravan, A.; Hayashi, H.; Tong, Y.; Infahsaeng, Y.; Chabera, P.; Pascher, T.; Yartsev, A. P.; Isoda, S.; Imahori, H.; Sundström, V. *J. Phys. Chem. C* **2013**, *117*, 6066−6080. (b) Hart, A. S.; KC, C. B.; Gobeze, H. B.; Sequeira, L. R.; D'Souza, F. *ACS Appl. Mater. Interfaces* **2013**, *5*, 5314−5323. (c) Imahori, H.; Kang, S.; Hayashi, H.; Haruta, M.; Kurata, H.; Isoda, S.; Canton, S. E.; Infahsaeng, Y.; Kathiravan, A.; Pascher, T.; Chabera, P.; Yartsev, A. P.; Sundström, V. *J. Phys. Chem. A* **2011**, *115*, 3679−3690.

(2) Mathew, S.; Yella, A.; Gao, P.; Humphry-Baker, R.; Curchod, B. F. E.; Ashari-Astani, N.; Tavernelli, I.; Rothlisberger, U.; Nazeeruddin, M. K.; Grätzel, M. *Nat. Chem.* **2014**, *6*, 242−247.

(3) (a) Nowak-Król, A.; Łukasiewicz, Ł. G.; Haley, J. E.; Drobizhev, M.; Rebane, A.; Cooper, T. M.; Gryko, D. T. *J. Porphyrins Phthalocyanines* **2014**, *18*, 998−1013. (b) Uetomo, A.; Kozaki, M.; Suzuki, S.; Yamanaka, K.-i.; Ito, O.; Okada, K. *J. Am. Chem. Soc.* **2011**, *133*, 13276−13279. (c) Wilson, G. S.; Anderson, H. L. *Synlett* **1996**, *11*, 1039−1040.

(4) (a) Loew, N. L.; Dzyuba, E. V.; Brusilowskij, B.; Kaufmann, L.; Franzmann, E.; Maison, W.; Brandt, E.; Aicher, D.; Wiehe, A.; Schalley, C. A. *Beilstein J. Org. Chem.* **2012**, *8*, 234−245. (b) Hatano, J.; Obata, N.; Yamaguchi, S.; Yasuda, T.; Matsuo, Y. *J. Mater. Chem.* **2012**, *22*, 19258−19263. (c) Samarat, A.; Kuninobu, Y.; Takai, K. *Synlett* **2011**, *15*, 2177−2180. (d) Berlicka, A.; Latos-Grazynski, L.; Lis, T. *Inorg. Chem.* **2005**, *44*, 4522−4533.

(5) (a) Bromby, A. D.; Keller, S. N.; Bozek, K. J. A.; Williams, V. E.; Sutherland, T. C. *J. Org. Chem.* **2015**, *80*, 9401−9409. (b) Kuo, M.-C.; Li, L.-A.; Yen, W.-N.; Lo, S.-S.; Lee, C.-W.; Yeh, C.-Y. *Dalton Trans.* **2007**, *14*, 1433−1439. (c) Screen, T. E. O.; Lawton, K. B.; Wilson, G. S.; Dolney, N.; Ispasoiu, R.; Goodson, T., III; Martin, S. J.; Bradley, D. D. C.; Anderson, H. L. *J. Mater. Chem.* **2001**, *11*, 312−320. (d) Spence, J. D.; Lash, T. D. *J. Org. Chem.* **2000**, *65*, 1530−1539. (e) McEwan, K. J.; Bourhill, G.; Robertson, J. M.; Anderson, H. L. *J. Nonlinear Opt. Phys. Mater.* **2000**, *9*, 451−468. (f) Lacey, J. A.; Phillips, D.; Milgrom, L. R.; Yahioglu, G.; Rees, R. D. *Photochem. Photobiol.* **1998**, *67*, 97−100. (g) Anderson, H. L.; Wylie, A. P.; Prout, K. *J. Chem. Soc., Perkin Trans. 1* **1998**, *10*, 1607−1611. (h) Milgrom, L.; Yahioglu, G.; Bruce, D. W.; Morrone, S.; Henari, F. Z.; Blau, W. J. *Adv. Mater.* **1997**, *9*, 313−316. (i) Milgrom, L. R.; Yahioglu, G. *Tetrahedron Lett.* **1996**, *37*, 4069−4072.

(6) Matsunaga, S.; Endo, N.; Mori, W. *Eur. J. Inorg. Chem.* **2011**, *29*, 4550−4557.

(7) Shen, Z.; Uno, H.; Shimizu, Y.; Ono, N. *Org. Biomol. Chem.* **2004**, *2*, 3442−3447.

(8) Luo, P.; Karsenti, P.-L.; Brisard, G.; Marsan, B.; Harvey, P. D. *Chem. Commun.* **2015**, *51*, 17305−17308.

(9) Harvey, P. D.; Mugnier, Y.; Lucas, D.; Evrard, D.; Lemaitre, F.; Vallat, A. *J. Cluster Sci.* **2004**, *15*, 63−90.

(10) (a) Salomon, C.; Dal Molin, S.; Fortin, D.; Mugnier, Y.; Boere, R. T.; Juge, S.; Harvey, P. D. *Dalton Trans.* **2010**, *39*, 10068−10075. (b) Dal Molin, S.; Mugnier, Y.; Fortin, D.; Harvey, P. D. *Dalton Trans.* **2010**, *39*, 8976−8981. (c) Lemaitre, F.; Lucas, D.; Groison, K.; Richard, P.; Mugnier, Y.; Harvey, P. D. *J. Am. Chem. Soc.* **2003**, *125*, 5511−5522. (d) Lemaitre, F.; Lucas, D.; Mugnier, Y.; Harvey, P. D. *J. Org. Chem.* **2002**, *67*, 7537−7540. (e) Brevet, D.; Lucas, D.; Cattey, H.; Lemaitre, F.; Mugnier, Y.; Harvey, P. D. *J. Am. Chem. Soc.* **2001**, *123*, 4340−4341. (f) Gauthron, I.; Mugnier, Y.; Hierso, K.; Harvey, P. D. *Can. J. Chem.* **1997**, *75*, 1182−1187.

(11) (a) Salomon, C.; Fortin, D.; Darcel, C.; Jugé, S.; Harvey, P. D. *J. Cluster Sci.* **2009**, *20*, 267−280. (b) Provencher, R.; Aye, K. T.; Drouin, M.; Gagnon, J.; Boudreault, N.; Harvey, P. D. *Inorg. Chem.* **1994**, *33*, 3689−3699.

(12) Aly, S. M.; Ayed, C.; Stern, C.; Guilard, R.; Abd-El-Aziz, A. S.; Harvey, P. D. *Inorg. Chem.* **2008**, *47*, 9930−9940.

(13) (a) Jeong, S.-D.; Min, B.; Cho, S. Y.; Lee, C.; Park, B. K.; An, K.-S.; Lim, J. *J. Org. Chem.* **2012**, *77*, 8329−8331. (b) Filatov, M. A.; Lebedev, A. Y.; Vinogradov, S. A.; Cheprakov, A. V. *J. Org. Chem.* **2008**, *73*, 4175−4185. (c) Filatov, M. A.; Cheprakov, A. V.; Beletskaya, I. P. *Eur. J. Org. Chem.* **2007**, *2007*, 3468−3475. (d) Borek, C.; Hanson, K.; Djurovich, P. I.; Thompson, M. E.; Aznavour, K.; Bau, R.; Sun, Y.; Forrest, S. R.; Brooks, J.; Michalski, L.; Brown, J. *Angew. Chem.* **2007**, *119*, 1127−1130.

(14) Yen, W.-N.; Lo, S.-S.; Kuo, M.-C.; Mai, C.-L.; Lee, G.-H.; Peng, S.-M.; Yeh, C.-Y. *Org. Lett.* **2006**, *8*, 4239−4242.

(15) Lindsey, J. S.; Schreiman, I. C.; Hsu, H. C.; Kearney, P. C.; Marguerettaz, A. M. *J. Org. Chem.* **1987**, *52*, 827−836.

(16) (a) Silva, S.; Pereira, P. M. R.; Silva, P.; Paz, F. A. A.; Faustino, M. A. F.; Cavaleiro, J. A. S.; Tomé, J. P. C. *Chem. Commun.* **2012**, *48*, 3608−3610. (b) Liu, L.; Fortin, D.; Harvey, P. D. *Inorg. Chem.* **2009**, *48*, 5891−5900.

(17) Gauthron, I.; Mugnier, Y.; Hierso, K.; Harvey, P. D. *Can. J. Chem.* **1997**, *75*, 1182−1187.

(18) Brevet, D.; Lucas, D.; Mugnier, Y.; Harvey, P. D. *J. Cluster Sci.* **2006**, *17*, 5−12.

(19) Connors, K. A. *Binding Constants: The Measurement of Molecular Complex Stability*; Wiley: New York, 1987.

(20) Makarska-Bialokoz, M. *J. Lumin.* **2014**, *147*, 27−33.

(21) Acar, M.; Bozkurt, E.; Meral, K.; Arik, M.; Onganer, Y. *J. Lumin.* **2015**, *157*, 10−15.

(22) Provencher, R.; Harvey, P. D. *Inorg. Chem.* **1996**, *35*, 2113−2118.

(23) Yu, H.-Z.; Baskin, J. S.; Zewail, A. H. *J. Phys. Chem. A* **2002**, *106*, 9845−9854.

(24) (a) Manojlovic-Muir, L.; Muir, K. W.; Lloyd, B. R.; Puddephatt, R. J. *J. Chem. Soc., Chem. Commun.* **1983**, *22*, 1336−1337. (b) Anderson, H. L. *Tetrahedron Lett.* **1992**, *33*, 1104−1104. (c) Sommer, J. R.; Shelton, A. H.; Parthasarathy, A.; Ghiviriga, I.; Reynolds, J. R.; Schanze, K. S. *Chem. Mater.* **2011**, *23*, 5296−5304. (d) Yamada, H.; Kushibe, K.; Okujima, T.; Uno, H.; Ono, N. *Chem. Commun.* **2006**, *4*, 383−385. (e) Suchy, P.; Dvorak, D.; Havelkova, M. *Collect. Czech. Chem. Commun.* **1999**, *64*, 119−129.

(25) (a) Du, B.; Stern, C.; Harvey, P. D. *Chem. Commun.* **2011**, *47*, 6072−6074. (b) Rochford, J.; Chu, D.; Hagfeldt, A.; Galoppini, E. *J. Am. Chem. Soc.* **2007**, *129*, 4655−4665.

(26) Frisch, M. J.; et al. *Gaussian 09*; Gaussian, Inc.: Wallingford, CT, 2004.

(27) Hohenberg, P.; Kohn, W. *Phys. Rev.* **1964**, *136*, B864−871.

(28) Hohenberg, P.; Kohn, W. *J. Phys. Rev.* **1965**, *140*, A1133−1138.

(29) Parr, R. G.; Yang, W. *Density-Functional Theory of Atoms and Molecules*; Oxford Univ. Press: Oxford, 1989.

(30) Salahub, D. R.; Zerner, M. C. *The Challenge of d and f ElectronsAm. Chem. Soc.*; American Chemical Society: Washington, D.C., 1989.*394*ix10.1021/bk-1989-0394.pr001

(31) Bauernschmitt, R.; Ahlrichs, R. *Chem. Phys. Lett.* **1996**, *256*, 454−464.

(32) Casida, M. E.; Jamorski, C.; Casida, K. C.; Salahub, D. R. *J. Chem. Phys.* **1998**, *108*, 4439−4449.

(33) Stratmann, R. E.; Scuseria, G. E.; Frisch, M. J. *J. Chem. Phys.* **1998**, *109*, 8218−8224.

(34) Lee, C.; Yang, W.; Parr, R. G. *Phys. Rev. B: Condens. Matter Mater. Phys.* **1988**, *37*, 785−789.

(35) Miehlich, B.; Savin, A.; Stoll, H.; Preuss, H. *Chem. Phys. Lett.* **1989**, *157*, 200−206.

(36) Becke, A. D. *J. Chem. Phys.* **1993**, *98*, 5648−5652.

(37) Binkley, J. S.; Pople, J. A.; Hehre, W. J. *J. Am. Chem. Soc.* **1980**, *102*, 939−947.

(38) Gordon, M. S.; Binkley, J. S.; Pople, J. A.; Pietro, W. J.; Hehre, W. J. *J. Am. Chem. Soc.* **1982**, *104*, 2797−2803.

(39) Pietro, W. J.; Francl, M. M.; Hehre, W. J.; Defrees, D. J.; Pople, J. A.; Binkley, J. S. *J. Am. Chem. Soc.* **1982**, *104*, 5039−5048.

(40) Dobbs, K. D.; Hehre, W. J. *J. Comput. Chem.* **1986**, *7*, 359−378.

(41) Dobbs, K. D.; Hehre, W. J. *J. Comput. Chem.* **1987**, *8*, 861−879.

(42) Dobbs, K. D.; Hehre, W. J. *J. Comput. Chem.* **1987**, *8*, 880−893.

(43) O'Boyle, N. M.; Tenderholt, A. L.; Langner, K. M. *J. Comput. Chem.* **2008**, *29*, 839−845.

DOI: 10.1021/acs.organomet.6b00050
*Organometallics* XXXX, XXX, XXX−XXX